Universal Dissipation Scaling for Nonequilibrium Turbulence

P. C. Valente* and J. C. Vassilicos†

Turbulence, Mixing and Flow Control Group, Department of Aeronautics, Imperial College London, London, United Kingdom‡

(Received 21 December 2011; published 23 May 2012)

It is experimentally shown that the nonclassical high Reynolds number energy dissipation behavior, $C_\varepsilon \equiv \varepsilon L/u^3 = f(\mathrm{Re}_M)/\mathrm{Re}_L$, observed during the decay of fractal square grid-generated turbulence (where Re_M is a global inlet Reynolds number and Re_L is a local turbulence Reynolds number) is also manifested in decaying turbulence originating from various regular grids. For sufficiently high values of the global Reynolds numbers Re_M, $f(\mathrm{Re}_M) \sim \mathrm{Re}_M$.

DOI: 10.1103/PhysRevLett.108.214503 PACS numbers: 47.27.Jv, 47.27.W−

In recent papers describing the wind tunnel turbulence generated by fractal square grids [1,2] it was shown that the turbulent kinetic energy dissipation rate, ε, at moderately high Reynolds numbers does not follow the expected scaling $\varepsilon L/u^3 \equiv C_\varepsilon \approx$ const (where L is the longitudinal integral length scale and u the streamwise rms velocity). Instead [1,2] found that $C_\varepsilon = f(\mathrm{Re}_M)/\mathrm{Re}_L$ during the turbulence decay where $f(\mathrm{Re}_M)$ is an increasing function of $\mathrm{Re}_M = U_\infty M/\nu$, a global Reynolds number based on a length scale M characteristic of the grid, and where $\mathrm{Re}_L = uL/\nu$ is a local, downstream position dependent, Reynolds number (ν is the kinematic viscosity and U_∞ is the inflow velocity). This behavior is accompanied by a well-defined power-law energy spectrum (with exponent close to Kolmogorov's $-5/3$) over a broad range of length scales and is therefore caused by a physically different underlying phenomenon than the well-known low Reynolds number law $C_\varepsilon \sim \mathrm{Re}_L^{-1}$.

Evidence of such a nonclassical behavior is significant due to the central role the empirical law $C_\varepsilon \approx$ const has on most, if not all, models and theories of both homogeneous and inhomogeneous turbulence [3–6]. Clearly, one should expect the existing models to inadequately describe turbulent flows (or regions thereof) not obeying the $C_\varepsilon \approx$ const scaling and, consequently, fail in their predictions of transport phenomena (energy transfer, dissipation, particle dispersion, scalar diffusion, etc.). Most importantly, it challenges our understanding of turbulence phenomena in general, nevertheless providing a starting point for its study as well.

In this Letter, we report results which show that this nonclassical behavior is in fact more general than previously thought and is not exceptional to the very special class of inflow conditions defined by fractal square grids. Hence this nonclassical behavior is of general scientific and engineering significance and therefore of much greater importance.

In the present experiments we compare turbulence generated by three different regular square-mesh grids (RG230, RG115, and RG60) with the turbulence generated by the fractal square grid (FSG) of [1] (see Fig. 1 and Table I). Our aim is to investigate the origin for the nonclassical dissipation behavior of the FSGs. The dimensions of RG230 are purposefully similar to those of the largest square on the FSG. This allows a *ceteris paribus* comparison between RG230 and FSG in two respects: (i) comparable inflow Reynolds numbers Re_M for similar inflow velocities if M is taken to be the side-length of the largest square on the grid (see Fig. 1), and (ii) comparable distance from the grid where the wakes of the RG230 bars meet and where the wakes of the FSG largest bars meet. Starting from any one of our grids, the turbulent kinetic energy increases as one moves downstream along the tunnel's center line and reaches a peak at a streamwise distance x_{peak} from the grid beyond which the turbulence decays [1,2,7]. This distance x_{peak} is closely related to the distance from the grid where the wakes (largest wakes in the case of FSG) meet. Indeed, [2] introduced the wake interaction length scale $x_* \equiv M^2/t_0$ where t_0 is the lateral thickness of the largest bars (see Fig. 1) and showed that x_{peak} scales with x_* in the case of FSGs. Subsequently, [1] showed that x_{peak}/x_* took comparable values for RGs and FSGs, a point which the experiments reported in this Letter allow us to confirm (see Table I). The length scales x_{peak} and x_* turn out to be paramount for a meaningful comparison between grids.

There are, of course, important differences between the four grids used here, for example, different values of blockage ratio σ (ratio between the blocking area of the grid and the area of the tunnel's test section) and different

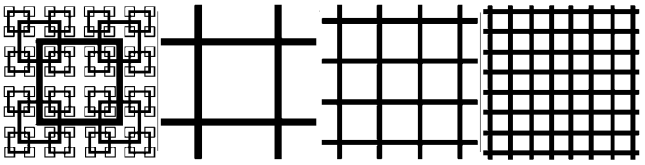

FIG. 1. Turbulence-generating grids. From left to right: FSG [1], RG230, RG115, and RG60.

 © 2012 American Physical Society

TABLE I. Details of turbulence-generating grids; d is the longitudinal thickness of the bars.

Grid		M (mm)	t_0 (mm)	d (mm)	σ (%)	x_* (m)	x_{peak}/x_*
RG230	Monoplanar	230	20	6	17	2.65	0.63
RG115	Monoplanar	115	10	3.2	17	1.32	0.63
RG60	Bi-planar	60	10	10	32	0.36	$\simeq 0.4$[a]
FSG	Monoplanar	237.7	19.2	5	25	2.94	0.45

[a]Taken from measurements of a very similar grid.

values of x_* (see Table I). These differences cause differences in various mean flow and turbulence profiles across the tunnel section. However, they have no baring on our main finding that the outstanding behavior previously found in FSG-generated turbulence is also present in turbulence generated by regular grids for a region whose extent is determined by x_*. Beyond this region, in the one case (RG60) where we can reach sufficiently far beyond it as a result of the wind tunnel's test section being much longer than x_*, we find the classical behavior $C_\varepsilon \approx$ const provided the Reynolds number is sufficiently high.

The experimental apparatus described in [1] was repeated for the present experiments with the length of the 0.46 m $\times$ 0.46 m-wide test section shortened from $\approx$ 4.5 m to $\approx$ 3.5 m to match the extent of the longitudinal traverse mechanism. We also installed a grid at the entrance of the diffuser to maintain a slight overpressure across the test section. All data are recorded with one- and two-component hot-wire anemometers operated at constant temperature. The main data are recorded with two in-house etched Pl-(10%)Rh single-wire (SW) sensors, SW1 and SW2, having sensing lengths of $l_w = 0.5$ mm and $l_w = 0.2$ mm and wire diameters of $d_w = 2.5$ μm and $d_w = 1$ μm, respectively. A Dantec 55P51 cross-wire (XW) with $l_w = 1.0$ mm and $d_w = 5$ μm is also used to record basic isotropy statistics. The spatial resolution of the measurements, quantified by l_w/η [$\eta \equiv (\nu^3/\varepsilon)^{1/4}$ is the Kolmogorov microscale; the isotropic estimate of dissipation $\varepsilon = 15\nu\overline{(du/dx)^2}$ is used], is given in Table II for the furthermost up- and downstream locations and for the different inflow velocities. We repeated the electronic tests to confirm that the maximum unattenuated frequency response of the SWs was at least $k\eta = 1$ (k is the wave number). The data acquisition and processing methodologies are also similar to those described in [1]. An exception is that we use, for simplicity, the classical Taylor's frozen field hypothesis to convert temporal into spatially varying signals, although we checked that this does not meaningfully affect the results.

This Letter's new data are recorded along the center line in the lee of each of our four grids (Fig. 1 and Tables I and II). Data recorded between a grid and its corresponding x_{peak} are excluded (see caption of Table II)

TABLE II. Overview of the experimental results. x_{min} & x_{max} are the first and last measurement locations corresponding to $0.48x_*$ & $1.09x_*$, $0.64x_*$ & $1.19x_*$, $0.61x_*$ & $2.38x_*$ and $0.72x_*$ & $8.75x_*$ for FSG, RG230, RG115 and RG60, respectively. Probe SW1 is used for the measurements of the first two grids and SW2 for the last two.

Grid	Symbol	U_∞ (ms^{-1})	Re_M ($\times 10^3$)	u/U_∞(%)	Re_λ x_{min}/x_{max}	l_w/η
FSG	⊠	15.0	237	9.7/5.0	385/249	4.8/3.0
	⊗	17.5	277		418/275	5.5/3.5
	◆	5.0	77	7.2/4.8	180/140	1.8/1.3
	□	10.0	153		261/200	2.9/2.2
RG230	●	15.0	230		326/258	3.9/3.0
	◇	17.5	268		348/281	4.4/3.3
	★	20.0	307		385/300	4.9/3.7
RG115	◈	20.0	153	6.9/2.7	255/160	2.3/1.1
RG60	◁	10.0	40	15/2.2	177/96	2.8/0.6
	▲	15.0	60		240/111	3.8/0.8
	▷	20.0	80		290/135	4.7/1.0

as we confine our study to decaying turbulence. In these decay regions, u/v (where v is the rms lateral velocity) is typically between 1.2 and 1.1 and the ratio of the mean square of the lateral turbulence velocity derivative with respect to the streamwise coordinate x to the mean square of the streamwise turbulence velocity derivative with respect to x takes values between 1.5 and 1.6. Both ratios vary by less than $\pm 5\%$ along the streamwise extent of our records. Note that x_{peak} is about as long as half the wind tunnel's extent in the cases of RG230 and FSG (see Table I). The RG60 was investigated in [1] where it was shown that for sufficiently high inlet velocities the dissipation followed a convincing $C_\varepsilon \approx$ const during decay far downstream. We repeat those measurements using a higher resolution sensor (SW2) and include recordings much closer to the grid (Table II).

First, we compare the dissipation scalings of the decaying turbulence originating from RG230 and FSG. The Reynolds numbers $\mathrm{Re}_\lambda \equiv u\lambda/\nu$ (where λ is the Taylor microscale) at our measurement stations are given in Table II and are all large enough for a significant separation to exist between the large, energy containing, eddies and the smallest dissipative eddies. Indeed, the scale separation at the highest Reynolds number is $L/\eta \approx 460$. The measured one-dimensional longitudinal energy spectra F_{11} exhibit clear power laws over more than a decade with an exponent close to Kolmogorov's $-5/3$, at least for $\mathrm{Re}_M \geq 2.3 \times 10^5$ and $\mathrm{Re}_\lambda \geq 250$ (see Fig. 2 where we only plot RG230 spectra for brevity and clarity; FSG spectra can be found in [1]). However, both for RG230 and SFG, the cornerstone assumption of turbulence theory, $C_\varepsilon \approx$ const, does not hold in this region where the turbulence decays

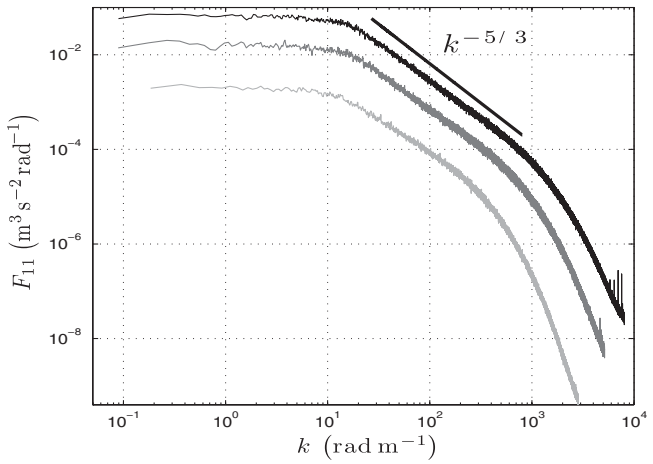

FIG. 2. Longitudinal energy density spectra F_{11} per wave number k of turbulence generated by RG230 for (black) $U_\infty = 20\ \mathrm{ms}^{-1}$, $x/x_* = 0.64$; (dark gray) $U_\infty = 10\ \mathrm{ms}^{-1}$, $x/x_* = 0.64$; and (light gray) $U_\infty = 5\ \mathrm{ms}^{-1}$, $x/x_* = 1.19$.

(between about 1.3 m from the grid and the end of the test section) at these Reynolds numbers (see Fig. 3). Instead, for any fixed Re_M, $C_\varepsilon \sim \mathrm{Re}_L^{-1}$ (as one moves along x) is a good qualitative approximation (in Fig. 3 each set of symbols corresponds to one Re_M and one grid, see Table II; Re_L decreases as x increases). At the furthest downstream locations which correspond to the lowest Re_L values for each Re_M in Fig. 3, there is a slight departure from $C_\varepsilon \sim \mathrm{Re}_L^{-1}$, probably due to far downstream test section confinement effects discussed in [1]. (In our records, L reaches a maximum value smaller than $M/4$ at $x_{\max}$ for all grids.) Note that the well-known relation $\varepsilon = 15\nu u^2/\lambda^2$ (e.g., [4]) and the definition of C_ε imply $15(L/\lambda)^2 = C_\varepsilon \mathrm{Re}_L$ and $15L/\lambda = C_\varepsilon \mathrm{Re}_\lambda$ which means that $C_\varepsilon \sim \mathrm{Re}_L^{-1}$ is

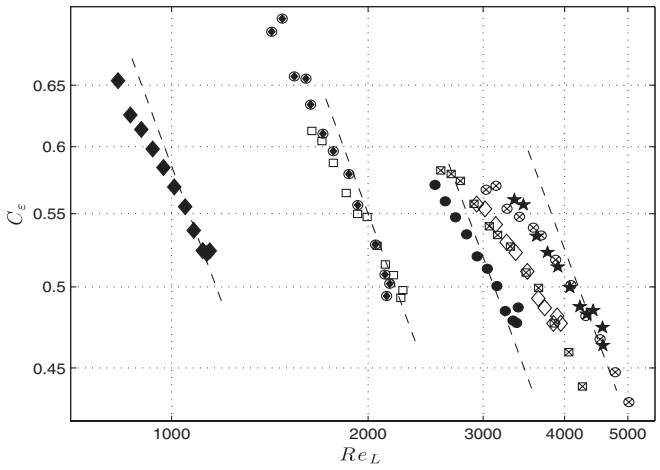

FIG. 3. Normalized energy dissipation C_ε versus local Reynolds number Re_L of turbulence generated by FSG, RG230 and RG115 for different inflow Reynolds numbers Re_M. The dashed lines follow $\propto \mathrm{Re}_L^{-1}$ for different Re_M. The Re_λ values of the data in this plot range between 140 and 418.

equivalent to $C_\varepsilon \sim \mathrm{Re}_\lambda^{-1}$ and that such C_ε behavior implies $L/\lambda \approx$ const during decay.

When, instead of keeping Re_M fixed and varying x, we keep x fixed and vary Re_M, we then find a very different dependence of C_ε on Reynolds number, asymptotically independent of it for both RG230 and FSG as Re_M increases. If we keep with the usual expectation that C_ε is independent of ν at high enough Re_M (which may be close to, but not exactly, true, see [8]), then these two different dependencies on Reynolds number can be reconciled by

$$C_\varepsilon \propto \frac{\mathrm{Re}_M}{\mathrm{Re}_L} \propto \frac{\mathrm{Re}_M^{1/2}}{\mathrm{Re}_\lambda} \tag{1}$$

because u/U_∞ and L/M are independent of Re_M to leading order at high enough Reynolds numbers. Note that $C_\varepsilon \propto \mathrm{Re}_M/\mathrm{Re}_L$ is equivalent to $L/\lambda \sim \mathrm{Re}_M^{1/2}$ and therefore to $C_\varepsilon \propto \mathrm{Re}_M^{1/2}/\mathrm{Re}_\lambda$. This equation is fairly well supported by our data both for FSG and RG230 at $\mathrm{Re}_M \geq 2.3 \times 10^5$ (Fig. 4) but with a grid-dependent constant of proportionality in (1).

Equation (1) may appear to clash with the fact that C_ε is approximately independent of both x and Re_M in the case of RG60 at distances greater than about 1.5 m from that grid in a wind tunnel test section of exact same width as the present one (see Fig. 7 in [1]). This is a distance greater than about $4x_*$ from the grid because $x_* \approx 0.36$ m for RG60. However, (1) has so far been established for decaying turbulence originating from RG230 and FSG up to downstream distances of less than about $1.5x_*$ (x_* takes much greater values for these grids, see Table I). It is therefore reasonable to investigate whether (1) and its equivalent relation $L/\lambda \sim \mathrm{Re}_M^{1/2}$ hold at distances below a few multiples of x_* from the RG60 grid. In Fig. 5 we plot L/λ as a function of the local Reynolds number Re_λ for RG60 at different levels of Re_M. We find that $L/\lambda \approx$ const

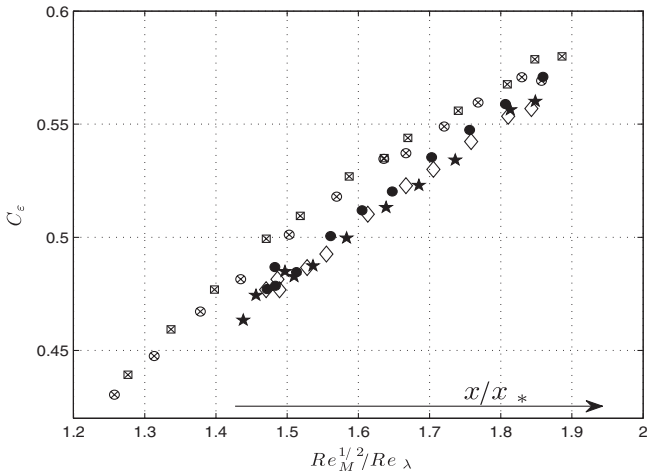

FIG. 4. Normalized energy dissipation C_ε versus the Reynolds number ratio $\mathrm{Re}_M^{1/2}/\mathrm{Re}_\lambda$ of turbulence generated by RG230 and FSG for different inflow Reynolds numbers Re_M.

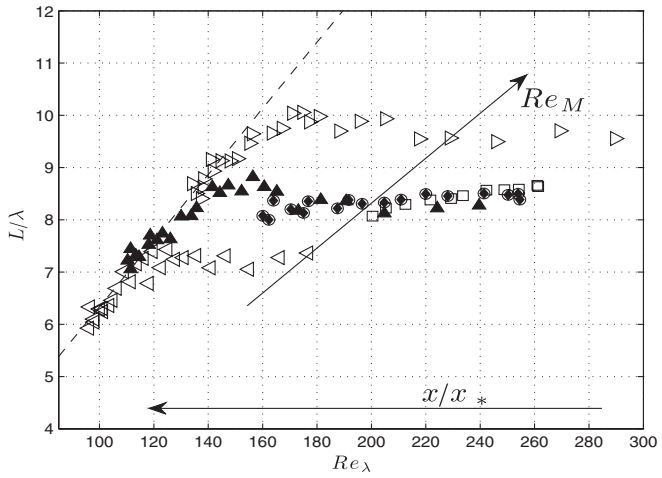

FIG. 5. L/λ versus the local Reynolds number Re_λ of turbulence generated by the RG60 for different Re_M and by RG115 and RG230 for the same Re_M. The dashed line follows $C_\varepsilon/15\,\mathrm{Re}_\lambda$ with $C_\varepsilon = 0.92$.

in the region between $0.72x_*$ and $2x_*$ (where Re_λ takes the largest values) and that L/λ and Re_λ decay in exact proportion to each other (i.e., $L/\lambda \sim \mathrm{Re}_\lambda$, which is equivalent to $C_\varepsilon = \text{const}$) at further downstream distances, i.e., where $x > 2x_*$. The region between $0.72x_*$ and $2x_*$ corresponds to the 10 highest Re_λ data points in Fig. 5 for each Re_M. The x-independent (therefore Re_λ-independent) value of L/λ in this region is an increasing function of Re_M as implied by (1). Such L/λ behavior was previously reported only for FSGs [1,2] and is now shown to be more general. Replotting the RG60 data so as to directly compare with (1), we obtain Fig. 6. Equation (1) is a fairly good representation of the data up to $\mathrm{Re}_M/\mathrm{Re}_L = 50$, i.e., in the turbulent decay region closest to the grid up to $x \approx 2x_*$. At streamwise distances larger than $2x_*$ where $\mathrm{Re}_M/\mathrm{Re}_L$ is larger than 50, C_ε becomes approximately independent

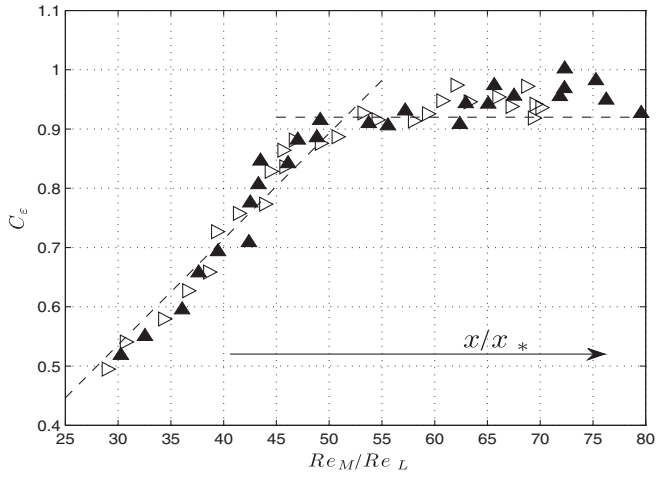

FIG. 6. Normalized energy dissipation C_ε versus the Reynolds number ratio $\mathrm{Re}_M/\mathrm{Re}_L$ of RG60-generated turbulence.

of both x and Re_M as already observed in earlier studies (e.g., [1]).

Our measurements of decaying turbulence originating from RG115 were designed for a direct comparison with RG230 at equal σ and $\mathrm{Re}_M = 1.53 \times 10^5$ but different mesh size M. The data obtained from these measurements are reported in Figs. 3 and 5 and show that L/λ and C_ε take effectively the same values for the two grids and that these values are consistent with $C_\varepsilon = f(\mathrm{Re}_M)/\mathrm{Re}_L$ and constant $L/\lambda = \sqrt{f(\mathrm{Re}_M)/15}$ in the ranges of x probed. However, Re_M is too low for (1) to hold.

The present data and those of [1,2] conspire to form the conclusion that, irrespective of the turbulence-generating grid (Fig. 1) and for high enough Re_M,

$$\varepsilon \approx C_1 \frac{U_\infty u^2}{L} \frac{M}{L} \tag{2}$$

and equivalently $L/\lambda \approx \sqrt{C_1 \mathrm{Re}_M/15}$ are acceptable approximations in the nonequilibrium decay region $x_{\mathrm{peak}} < x < x_e$ where $x_e \approx 2x_*$ for RG60 and C_1 is a dimensionless constant which only depends on inlet or boundary geometry (type of fractal or regular grid, σ, etc.). We might expect x_e to scale with x_* for other grids as well, and the equilibrium dissipation scaling $\varepsilon = C_2 u'^3/L$ (where C_2 is an inlet or boundary geometry-dependent dimensionless constant, see [8,9]) to be recovered at $x > x_e$ for other grids too. However, our RG115, RG230, and FSG data and those of [1,2] do not allow us to test these expectations, nor do they allow us to explore how x_e/x_* may depend on inlet or boundary conditions. RG230 and FSG, in particular, act as magnifying lenses which make the nonequilibrium region longer than the entire tunnel section's length. Equations (1) and (2), and more generally $C_\varepsilon = f(\mathrm{Re}_M)/\mathrm{Re}_L$ which also covers lower values of Re_M, are approximately true in the nonequilibrium region irrespective of flow and turbulence profile details which differ from grid to grid. The FSGs are magnifying lenses with added capabilities for tailoring flow and turbulence profiles which go beyond variations in σ.

Finally, it is important to stress that the energy spectrum has a well-defined power-law shape over nearly two decades with exponent close to $-5/3$ at the closest point to the grid that we sampled in the nonequilibrium region (Fig. 2). This power-law region becomes progressively narrower with an exponent progressively further away from $-5/3$ as x increases. In the equilibrium region of RG60 where $\varepsilon \sim u'^3/L$, the energy spectrum is far from Kolmogorov shaped. This may just be a consequence of the low Reynolds numbers in the equilibrium region of our RG60 runs. But it is remarkable that a near-Kolmogorov power-law shaped energy spectrum does in fact appear well before the turbulence has had the time to reach equilibrium. A similar observation was made in [10] where near-Kolmogorov power-law energy spectra were reported in a cylinder wake within one cylinder diameter from the cylinder.

We are grateful to Zellman Warhaft and Jose Cardesa-Duenas for stimulating discussions. P. C. V. acknowledges the financial support from Fundação para a Ciência e a Tecnologia (SFRH/BD/61223/2009, cofinanced by POPH/FSE).

*p.valente09@imperial.ac.uk
†j.c.vassilicos@imperial.ac.uk
‡www.imperial.ac.uk/tmfc

[1] P. C. Valente and J. C. Vassilicos, J. Fluid Mech. **687**, 300 (2011).
[2] N. Mazellier and J. C. Vassilicos, Phys. Fluids **22**, 075101 (2010).
[3] A. A. Townsend, *The Structure of Turbulent Shear Flow* (Cambridge University Press, Cambridge, 1956).
[4] H. Tennekes and J. L. Lumley, *A First Course in Turbulence* (MIT Press, Cambridge, New York, 1972).
[5] A. S. Monin and A. M. Yaglom, *Statistical Fluid Mechanics* (MIT Press, Cambridge, MA, 1975), Vol. II.
[6] U. Frisch, *Turbulence: The Legacy of A. N. Kolmogorov* (Cambridge University Press, Cambridge, 1995).
[7] Jayesh and Z. Warhaft, Phys. Fluids A **4**, 2292 (1992).
[8] N. Mazellier and J. C. Vassilicos, Phys. Fluids **20**, 015101 (2008).
[9] P. Valente and J. Vassilicos, Phys. Lett. A **376**, 510 (2012).
[10] M. Braza, R. Perrin, and Y. Hoarau, J. Fluids Struct. **22**, 757 (2006).